




Three-dimensional imaging of pharmaceutical tablets using serial sectioning and Raman chemical mapping

Hannah Carruthers^{1,2}  | Don Clark² | Fiona C. Clarke² | Karen Faulds¹  |
Duncan Graham¹ 

¹Department of Pure and Applied Chemistry, University of Strathclyde, Glasgow, UK

²Pfizer Ltd., Sandwich, UK

Correspondence

Duncan Graham, Department of Pure and Applied Chemistry, University of Strathclyde, George Street, Glasgow G1 1RD, UK.

Email: duncan.graham@strath.ac.uk

Funding information

Global Technology and Engineering, Pfizer Global Supply

Abstract

Chemical mapping by Raman spectroscopy is widely used in the pharmaceutical industry to characterise the distribution of components within pharmaceutical tablets; however, current methods do not go beyond examining an exposed surface area of a sample. There are known limitations with estimating domain size and shape statistics from 2D chemical images as the values obtained will depend on where the domain is sectioned, potentially under- or overestimating its true value. The combination of Raman spectroscopic mapping and serial sectioning has been recently explored as an alternative method to obtain a depth profile of a sample; however, to date, this has involved instrumentation capable of automated Raman mapping with subsequent sample sectioning. A key requirement for Raman mapping is producing an optically flat surface, and this becomes increasingly challenging for larger surface areas required for the examination of a pharmaceutical tablet. Here, we describe 3D imaging of a tablet matrix by combining Raman mapping with independent sample sectioning to provide appropriate lateral and axial resolution. The approach was first validated by analysing a spherical object of known size and shape and comparing the 3D domain size statistics calculated from the reconstructed image to its absolute values. The method was then applied to a three-component model system, simulating a pharmaceutical tablet, to determine the capability and applicability of the method for solid dosage formulations. The study demonstrated that relative differences in the size, shape and distribution of domains can be quantified enabling an enhanced understanding of the spatial arrangement of each component within the formulation and the effect of each processing condition on the final drug product. By visualising the 3D structure of a tablet matrix with demonstrable accuracy and precision using materials of known dimensions, new capabilities to enhance tablet manufacturing methods are now available.

KEYWORDS

3D imaging, chemical imaging, pharmaceutical tablets, Raman, serial sectioning

This is an open access article under the terms of the Creative Commons Attribution License, which permits use, distribution and reproduction in any medium, provided the original work is properly cited.

© 2022 The Authors. *Journal of Raman Spectroscopy* published by John Wiley & Sons Ltd.

1 | INTRODUCTION

Pharmaceutical tablets are the most widely used solid dosage form for the administration of therapeutic agents.¹ There are recognised knowledge gaps within current tablet manufacturing processes, particularly relating to the spatial distribution of components within the formulation. By fully understanding the microstructure of tablet matrices, manufacturing processes can be designed to deliver products with desired attributes. In this study, we explore an alternative three-dimensional (3D) Raman mapping technique to obtain qualitative and quantitative 3D structural information of a tablet system. To extend the current capabilities of two-dimensional (2D) spectroscopic mapping tools, a 3D representation of a components' distribution within a tablet can be obtained by acquiring 2D Raman chemical maps at regular penetration depths into the sample by physically milling the sample and examining the exposed surface. 3D reconstruction allows image planes orthogonal to the measured XY plane to be visualised enabling an enhanced understanding of the 3D structure of a tablet matrix.

There are several well-established techniques available that can generate high resolution images of a tablet's component distribution, but they generally cannot go beyond examining an exposed surface area. X-ray microtomography (XMT) is the main method for 3D imaging of pharmaceutical samples; however, the requirement for each component to exhibit a different X-ray attenuation coefficient makes this technique unsuitable for visualising the spatial distribution of components within pharmaceutical tablets. Many excipients are organic in nature and exhibit similar structures and densities making them difficult to differentiate by XMT. Instead, XMT is largely used for understanding structural features and how these may change during manufacturing, handling and storage.²

Raman and near-infrared (NIR) spectroscopic chemical imaging are widely used in the pharmaceutical industry for 2D chemical imaging of a tablet matrix.^{3–8} The combination of microscopy and spectroscopy enables the spatial distribution of components to be easily visualised. Pharmaceutical applications typically involve visualising and comparing differences in the size, shape and distribution of components to monitor process changes^{9,10} or understand out-of-specification (OOS) batches.¹¹ In our previous work, we compared the relative performance of Raman and NIR chemical imaging for the analysis of pharmaceutical tablets and demonstrated that Raman offers superior image quality with regard to visualising detailed domain morphology.⁵ Current methods, however, only involve examining a single 2D section of the sample and assume the image obtained is representative of the bulk tablet.^{12,13} Inhomogeneous or OOS samples can deviate from this assumption and should be taken into consideration when interpreting 2D chemical images.

Image processing plays a crucial role in pharmaceutical chemical imaging to further interpret the grey scale and/or red, green and blue (RGB) images generated. Domain size statistics can be calculated to assess the particle size of active pharmaceutical ingredients (APIs) and excipients within drug formulations.¹⁴ There are, however, known limitations associated with obtaining particle size and shape information from 2D images. The largest discrepancies are found when estimating the size and dimensions of spherical and cubic components, illustrated in Figure 1. The diameter of a spherical domain obtained from a 2D cross-section will depend on the depth at which the domain was sectioned, and thus, the true diameter of a spherical component will consistently be underestimated within a 2D chemical image.¹³ In contrast, if a cube is sectioned across the diagonal of one, or more, of its faces, its dimensions will be overestimated. The size, shape and dimensions of a particle can only

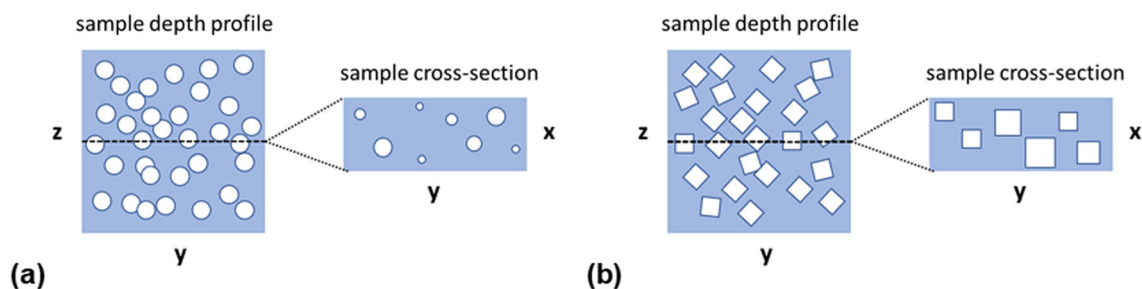


FIGURE 1 A schematic representation of a chemical image from a hyperspectral sample cross-section of a (a) sphere distribution and (b) cube distribution through a matrix where the size of spherical components is underestimated and cubic components overestimated. Figure adapted from Clark and Šašić¹³ [Colour figure can be viewed at wileyonlinelibrary.com]

ever be estimated from 2D chemical images. Movement to 3D chemical imaging would provide full visualisation of domain size and shape and could hold the key to an improved understanding of the complete structure of tablet matrices.

The combination of Raman imaging with confocal light collection has been widely explored as a method to obtain a depth profile of a specimen.^{15–18} Altering the focus enables chemical images to be obtained at various penetration depths into the sample. A 3D image of a sample may then be constructed by acquiring and combining a number of 2D chemical images at regular penetration depths into the sample. This method has been extensively explored for the analysis of polymeric films,¹⁹ silicates²⁰ and semiconductors.²¹ However, there are recognised limitations associated with this method as metallurgical objectives are still frequently used in many Raman microscopes.²² Metallurgical objectives are known to severely impact the quality of data obtained when focusing below the sample surface in the form of degraded spatial resolution, poorer signal-to-noise (S/N) and compression of depth scales.^{23,24} The capabilities of this technique to extend to 3D visualisation of pharmaceutical samples are also limited in large part by the maximum depth available for analysis. Review of the literature suggests the maximum depth of penetration available is typically $\sim 50\ \mu\text{m}$.^{15,16} The particle size of many APIs and excipients often exceeds this size range. For example, the common diluent, microcrystalline cellulose (MCC), has an average particle size of $\sim 100\ \mu\text{m}$.²⁵ The inability to extend this method to visualise a whole tablet matrix makes this method unsuitable for the analysis of solid dosage forms.

Serial section Raman tomography has been more recently explored as an alternative method to obtain a 3D image of a sample. The combination of sample sectioning with subsequent Raman mapping of the exposed surface area can overcome the challenges associated with confocal Raman depth profiling. Böhm et al.²⁶ demonstrated the successful use of this technique for 3D imaging polymer blends, reaching a maximum depth resolution of $100\ \mu\text{m}$. Muzzio and Panikar^{27,28} have also demonstrated

the use of this technology for 3D Raman imaging of a tablet microstructure and was used to characterise differences in the spatial distribution of components for a formulation manufactured by two different processing routes. Both examples involve instrumentation capable of automated sample milling with subsequent Raman mapping.

It is generally widely accepted that sample preparation is a crucial step in spectroscopic imaging experiments. The aim of sample sectioning is to produce a sample surface, which is optically flat and parallel to the incident radiation to ensure the sample does not drop out-of-focus as the sample stage moves. A comparison of sample preparation methods has recently been reported by Gupta et al.,²⁹ including automated sample grating. In this study, the surface quality of the sample after serial sectioning was not explored nor the capabilities of each technique for removing relatively small depths of material ($20\ \mu\text{m}$). As part of the preliminary work for this study, we evaluated a number of sample preparation techniques, including the cited methods, and concluded that milling was the most appropriate technique for consistently producing an optically flat surface after serial sectioning relatively small depths ($20\ \mu\text{m}$).

In this paper, we describe a method to overcome the limitations associated with using automated sample preparation for serial sectioning by manually preparing the sample before each Raman mapping experiment. A 3D image of the components distribution within a tablet matrix can then be reconstructed by stacking the individual 2D Raman chemical images collected at regular depths into the sample, illustrated in Figure 2. Our proposed method was first validated by performing a 3D experiment on a material of known size and shape. 3D domain size statistics such as volume and surface area were calculated from our reconstructed 3D data and compared with its absolute values to determine the capability and applicability of our method. A three-component system composed of an API and two excipients, simulating a real pharmaceutical tablet, was then explored to examine the added value of 3D chemical imaging for pharmaceutical tablets.

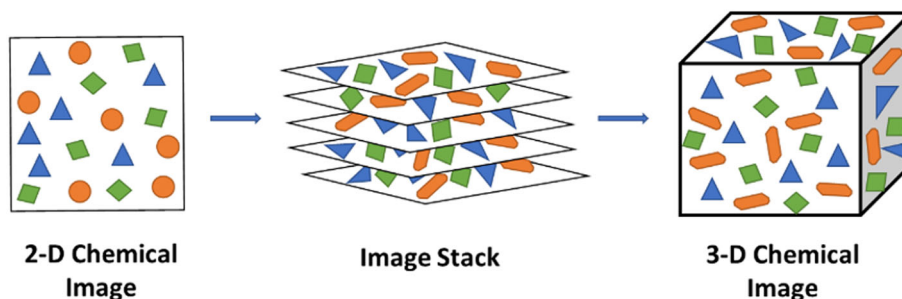


FIGURE 2 A schematic representation of the 3D chemical image construction process [Colour figure can be viewed at wileyonlinelibrary.com]

2 | EXPERIMENTAL

2.1 | 3D method validation AmberLite™ Na Ion Exchange Resin

The AmberLite™ Na Ion Exchange Resin (AmberLite™) was compacted within a wafer of the common diluent agent, MCC, in a 0.15:0.85 w/w ratio, respectively. The raw materials were weighed using a METTLER TOLEDO® XP205 analytical balance, and the combined mixture was blended using a TURBULA® shaker-mixer (Glen Mills Inc, New Jersey, USA) at a rate of 46 rotations per minute for 5 min. A Specac Atlas Auto T8 wafer press (Specac Ltd, Orpington, UK) was used to compact the blend into a wafer. An A2 scoop (1.25 mL) of the formulation was inserted into a 10 mm die and compressed to 1 tonne, held for one minute and medium release to 0 tonne.

2.1.1 | Sample preparation

To ensure the exact same XY position of specimen was examined after each milling procedure, the sample was mounted onto a chemical image fusion microscope slide^{5,13,30} containing four crosshair markers. The coordinate markers enable relocation to the exact same sample area if there was any minor movement in the position of the microscope slide relative to the Raman mapping instrument post milling.

A Leica EM Rapid Tablet Mill was used to remove 20 µm of material from the sample after each Raman mapping experiment. Generally, the milling procedure included a polishing step size of 2 µm that was repeated 10-fold. If required, this procedure could be amended in real time to improve the surface quality of the compact to produce an optically flat surface suitable for chemical imaging. The depth of the sample was measured before and after sectioning using a micrometre (Mitutoyo Ltd., Hampshire, UK) to ensure the exact desired depth had been removed between each experiment.

2.1.2 | Raman mapping data collection

All Raman data were collected using a WITec Alpha 500+ CRM (WITec GmbH, Ulm, Germany) Raman microscope with a 50× 0.80 NA glass objective, charge-coupled device (CCD) detector, equipped with a 785 nm laser excitation source. The sample was mounted on a motorised XYZ stage, and spectra were acquired with a 0.1 s data acquisition time. The instrument operates a spectral range of 132.5–1910 cm⁻¹ with a spectral

resolution of 1 µm. A step size of 20 µm was chosen in both the X and Y direction to be the same as each z-slice milled. Each spectrum obtained represents a cubic voxel in 3D space with the dimensions of 20 µm (x) × 20 µm (y) × 20 µm (z). A 600 µm (x) by 600 µm (y) sample area was measured to ensure the whole resin bead would be included in the chemical map.

The resin bead analysed in this experiment was located within the MCC compact by milling the sample using a Leica EM Rapid Tablet Mill (Leica, Wetzlar, Germany) and examining the exposed surface using the light microscope equipped to the Raman mapping instrument. Depth increments of 20 µm were removed from the sample until the pinnacle of an AmberLite™ bead could be visualised. Here, the Raman mapping area for the 3D experiment was defined, and the first 2D Raman chemical map was acquired.

2.1.3 | 2D chemical image data processing

2D chemical images were prepared using ISys® 5.0 chemical imaging software. Single channel images of the AmberLite™ component were prepared by univariate analysis. Spectral comparison of AmberLite™ with MCC revealed AmberLite™ exhibits a unique, sharp Raman band at 1601 cm⁻¹ suitable for univariate analysis, which we attribute to the aromatic ring C=C stretching vibration.³¹

2.1.4 | 3D visualisation and domain size statistics

Fiji^{32,33} image processing software was employed to generate an image stack of the 2D single channel images. The 3D Viewer plugin³⁴ was used to visualise the image stack in 3D space as volumes and orthoslices. 3D quantitative domain size statistics were calculated using the 3D Object Counter plugin³⁵ within the Fiji image processing software. First the image stack was separated into individual stacks of each component. Each image stack was binarised and underwent a 2-pass connectivity analysis method to identify discrete objects in 3D. Each binary image was scanned from the top left-hand corner to the bottom right-hand corner. When a pixel with a value of 1 was identified, it was assigned with a tag. All neighbouring pixels, including pixels on the adjacent 2D chemical images, were checked for an existing tag. The second scan enabled all ambiguities to be resolved, for example, a u-shaped object only connected by its bottom parts may be tagged separately in the first pass however can be identified as a single object in the second. This built a 3D

representation of all domains for a particular component. Quantitative domain size statistics such as volume and surface area were easily calculated for each object by its number of voxel pixels.

2.2 | 3-component model system

2.2.1 | 1:1:1 formulation

The sample compact was composed of a three-component formulation containing an active ingredient (eletriptan hydrobromide), a common diluent agent (MCC) and a secondary excipient (saccharin) in a 1:1:1 w/w ratio. The model compact was prepared using the same method described for the MCC:AmberLite™ wafer.

2D Raman chemical images were acquired at 30 μm depth intervals into the sample by physically milling the surface using a Leica EM Rapid Tablet Mill (Leica, Wetzlar, Germany). The same sample milling procedure described for the AmberLite™ 3D study was used for this experiment.

All Raman data were collected using the same instrument and data acquisition parameters used for the AmberLite™ 3D study. For each 2D chemical image, a sample area of 3000 μm (x) by 3000 μm (y) was measured. A total number of 84 2D chemical images were acquired corresponding to a dataset with the total volume of 3000 μm (x) × 3000 μm (y) × 2490 μm (z).

2.2.2 | 0.80:0.15:0.05 formulation

A sample compact composed of eletriptan hydrobromide, MCC and saccharin in a 0.05:0.80:0.15 w/w ratio was prepared using the same wafer preparation methods previously described. 2D Raman chemical images were obtained at 20 μm depth intervals into the sample by physically milling the surface using the same milling procedure described for the previous 3D studies.

All Raman data were collected using the same instrument and data acquisition parameters used for the previous experiments. For each 2D chemical image, a sample area of 500 μm (x) by 500 μm (y) was measured. A total number of 26 2D chemical images were acquired corresponding to a dataset with the total volume of 500 μm (x) × 500 μm (y) × 500 μm (z).

2.2.3 | 2D chemical image data processing

2D chemical images were produced using ISys® 5.0 chemical imaging software. All datasets were treated with

partial least squares-discriminant analysis II (PLS-DA II) using a reference library of the raw materials. The library was built by acquiring 1000 × 1000 μm pure Raman maps of each component and was used to construct a PLS classification model. Application of the PLS-DA II model to 2D Raman data resulted in a classification score image for each component where the intensity of each pixel is determined by its degree of membership to that particular component. Spectral comparison of the response at a given pixel with the reference library spectra determines its degree of membership to each class and is assigned an arbitrary value between 0 and 1. A score value of 0 demonstrates the absence of a component in a pixel, and score value of 1 represents 100% presence of a component. RGB images representing the spatial arrangement of components for each 2D dataset were obtained by combining the classification images for each component.

2.2.4 | 3D visualisation and domain size statistics

3D visualisation and domain size statistics were obtained by using the methods previously described for the AmberLite™ 3D study.

3 | RESULTS AND DISCUSSION

3.1 | Domain size statistics validation AmberLite™ Na Ion Exchange Resin

A 3D Raman mapping experiment was conducted on a material of known size and shape to validate our proposed 3D imaging method. AmberLite™ Na Ion Exchange Resin (C₁₃H₁₀ClNO₄S) was chosen due to its spherical morphology and strong Raman response (Figure 3), enabling its 3D dimensions to be easily determined and compared with statistics calculated from the reconstructed 3D image.

The AmberLite™ Na Ion Exchange Resin was embedded within a compact of MCC (C₁₄H₂₆O₁₁) to replicate the sample and sectioning procedure that would be required for a 3D Raman mapping experiment of a pharmaceutical tablet. A z-slice size of 20 μm was chosen as a compromise between being significantly smaller than the primary particle size of the Amberlite™ bead to obtain detailed morphological information and allow a fast 3D data acquisition time. Both components differ in their chemical nature and can be uniquely identifiable by Raman spectroscopy. The structures of each material and their respective Raman spectra are displayed in Figure 3b.

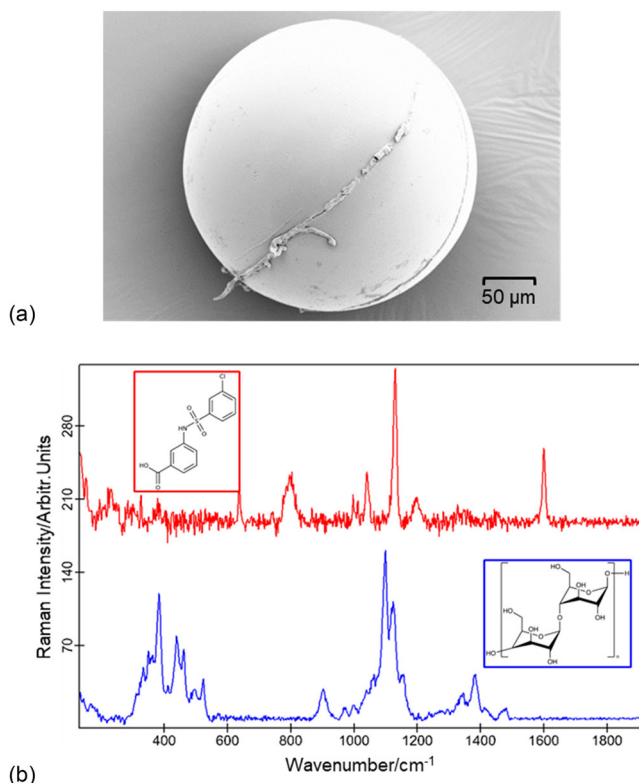


FIGURE 3 (a) A scanning electron micrograph of AmberLite™ Na Ion Exchange Resin at 250 \times and (b) the molecular structure and Raman spectrum of (top) AmberLite™ Na Ion Exchange Resin and (bottom) microcrystalline cellulose (MCC) obtained using a 785 nm excitation laser with a 0.5 s acquisition time [Colour figure can be viewed at wileyonlinelibrary.com]

3.2 | AmberLite™ Na Ion Exchange Resin 3D experiment

The reconstructed volumetric 3D Raman map of the AmberLite™ bead obtained using FIJI 3D Viewer³⁴ plugin is shown in Figure 4. The individual 2D univariate images used for the 3D reconstruction can be found in the supplementary material (Figure S1). The small fragments of AmberLite™ surrounding the large primary bead were removed prior to performing further image processing and 3D domain size analysis.

Visual inspection of the 3D volume reveals a spherical-like shaped object consistent with the morphology of the AmberLite™ raw material. This observation preliminarily suggests that the 3D mapping method described in this paper is suitable to visualise the 3D shape of discrete particles. Closer inspection reveals the surface area of the bead appears slightly irregular, differing from the smooth surfaces shown in the SEM micrograph of the raw material (Figure 3). A chemical mapping dataset consists of an array of spectral data

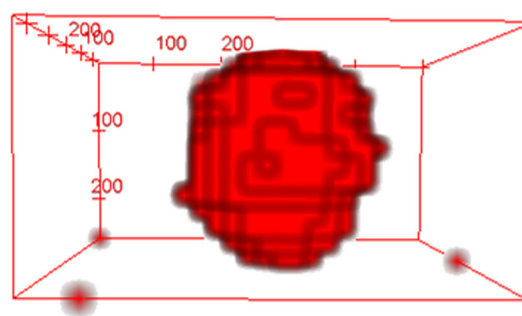


FIGURE 4 A 3D volumetric representation of the AmberLite™ Na Ion Exchange Resin bead reconstructed using FIJI 3D Viewer³⁴ software from 2D Raman chemical maps obtained at regular depth intervals. The red pixels represent a Raman response at 1601 cm^{-1} (a unique wavenumber for AmberLite™ Na Ion Exchange Resin). The 2D Raman chemical maps were collected using a 785 nm excitation laser with a 0.5 s acquisition time and a 20 μm XYZ spatial step size [Colour figure can be viewed at wileyonlinelibrary.com]

points with known spatial location. Data processing methods treat each data point as adjacent even if the sample step size is larger than the sample spot size.¹³ The resultant RGB chemical image is therefore composed of a number of square shaped pixels; therefore, producing chemical images of circular and spherical shaped objects with characteristically smooth boundaries cannot always be achieved.

To further validate the 3D mapping method, quantitative 3D domain size statistics were calculated from the reconstructed 3D image and compared with its measured spherical value from SEM. The resin bead may not be perfectly spherical, which could introduce some error in the calculated value. Due to the formulation preparation methods used, it is not possible to determine the exact resin bead that was examined in the 3D experiment, and its size, shape and dimensions cannot be characterised prior to analysis. Characterisation of the resin raw material (Figure 3a) reveals the beads are spherical in shape and suggest that this is a reasonable assumption to make.

The maximum Feret diameter (272 μm) obtained from 2D domain size analysis of the individual 2D chemical maps was used to calculate the volume and surface area of the examined bead. Comparison of the maximum Feret diameter (272 μm) with the z-depth calculated from the number of chemical images containing a AmberLite™ Raman response (260 μm) reveals comparable diameters for the examined bead further validating the 3D method. The small discrepancy between the two values is due to the inability to determine the precise starting location of an object of interest between two consecutive chemical images where a Raman response is first detected in the second image. An XYZ spatial step size of

20 μm , chosen for this experiment, introduces an error of $\pm 20 \mu\text{m}$ in the radius of the object of interest measured in both the XY plane and z-projection. A comparison of the diameter calculated and 3D Object Counter calculated values for the examined AmberLite™ bead is shown in Table 1.

The volume calculated from the 3D image using the 3D Object Counter plugin³⁵ slightly underestimates its true value by $\sim 20\%$. The z step size chosen in a 3D experiment will introduce some error in the quantitative statistics calculated due to potentially underestimating the beads of interests true depth. For this example, the z-depth of the AmberLite™ Na Ion Exchange Resin bead appears to be slightly underestimated, and thus, the volume of the reconstructed object is also underestimated. Errors may be decreased by reducing the z step size chosen for the 3D experiment. The z step size used in a 3D experiment is determined by a combination of the primary particle size of the material to be examined as well as the number of chemical images required to build a 3D dataset and its associated data acquisition time. For a particle in the range of $\sim 300 \mu\text{m}$, a z step size of $20 \mu\text{m}$ is sufficient to determine relative 3D differences between particles.

The surface area calculated from the reconstructed 3D chemical image slightly overestimates its true surface area. Inspection of the 3D volume representation of the examined bead in Figure 4 reveals an object with an irregular surface consistent with an overestimated surface area. The irregular boundary present highlights one of the main challenges associated with mapping circular/spherical domains. A chemical imaging dataset is composed of a 2D array of data points containing both spatial

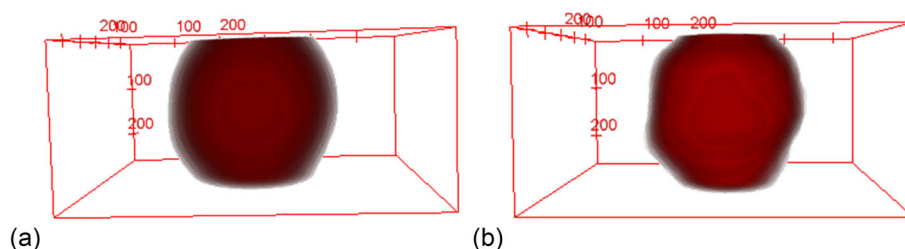
and spectral information. Image processing classifies each point to belong to a particular component and is visualised as a chemical image composed of square-shaped pixels. Each domain displayed within a chemical image will be composed of many pixels. Circular domains can therefore not be represented in chemical images by its characteristic round shape with smooth edges and instead will be represented by an object with an irregular boundary. Irregularities may be reduced by lowering the XY spatial step size; however, the lateral spatial resolution chosen for a chemical mapping experiment is usually largely influenced by the primary particle size of the material to be examined as well as its associated data acquisition time. Typically, for 3D serial sectioning imaging experiments, an equivalent Z and XY spatial step size is chosen to ensure the same spatial error in 3D. Lowering the XY spatial step size significantly increases the data acquisition time and may not contribute any further useful information regarding domain morphology. Instead, morphological filters may be applied to 2D or 3D chemical images to blur or smooth domain boundaries.

To further improve the 3D visual representation and accuracy of the 3D domain size statistics calculated from reconstructed image, a series of 3D image filters were explored to smooth and blur the object boundary. A Gaussian Blur (also known as Gaussian Smoothing) filter applies a 3D Gaussian smoothing kernel to a 3D image. The degree of smoothing is determined by the standard deviation of the Gaussian. The output is a weighted average of each pixels' neighbourhood, with the heaviest weighting (highest Gaussian value) towards the central pixels. When applied in three dimensions, the output is a surface whose contours are concentric spheres with a Gaussian distribution from the centre point. A mean filter is similar to a Gaussian blur filter but instead uses an ellipsoidal kernel. The degree of smoothing is determined by the radius of the kernel. Each pixel is replaced by the average value of its neighbours, including itself. Pixel values unrepresentative of their surrounding are eliminated. Mean filtering is most commonly used as a method of noise reduction and “softens” object boundaries by decreasing high frequency detail. The 3D volume representation of the filtered datasets is displayed in Figure 5.

TABLE 1 A comparison of the diameter calculated and 3D Object Counter calculated values for the AmberLite™ Na Ion Exchange Resin bead

	Volume/ $\times 10^6 \mu\text{m}^3$	Surface area/ $\times 10^4 \mu\text{m}^2$
Diameter calculated	10.5	23.2
3D Object Counter	8.32	29.3
% Difference	-20.8	+26.2

FIGURE 5 A 3D volume representation of the AmberLite™ Na Ion Exchange Resin bead processed by (a) 3D Gaussian Blur and (b) 3D Mean filter [Colour figure can be viewed at wileyonlinelibrary.com]



Visual inspection of the filtered volumetric 3D maps reveals objects with smoother boundaries, more characteristic to a sphere. However, the reconstructed images show some deviations from the perfectly spherical object suggested by the raw material, such that the top and bottom of the object appear to be flat, particularly for the 3D Gaussian Blur processed data. As discussed earlier, our proposed method introduces some error as the exact starting location of an object of interest between two consecutive chemical images cannot be determined, and therefore, it is possible that the top and bottom of the Amberlite™ bead may not be observed in the 2D chemical images obtained resulting in a reconstructed 3D image with a flat top and bottom. This effect has been exaggerated in the processed data compared with the raw reconstructed image and thus will introduce some error into any 3D domain size statistics calculated.

To determine if the filtering methods improve the accuracy of the 3D domain size statistics calculated from reconstructed images, 3D domain size statistics were calculated from the processed data. A comparison of the calculated 3D domain size statistics determined from the filtered datasets with the raw and diameter calculated values is shown in Table 2.

The volume calculated from the processed datasets is more comparable with its diameter calculated value suggesting that some errors are introduced from the irregular boundaries created by the chemical mapping method. The difference in values between the raw and processed data is, however, small suggesting that 3D filtering may not be necessary to determine relative differences in the size and shape of domains. Instead, the majority of errors may be due to the method itself and therefore will be systematic for all datasets, if method parameters remain constant. 3D domain size statistics can therefore be easily compared across components and datasets to determine relative differences in the size, shape and distribution of a particular component. This experiment also studies the most difficult shaped object to characterise via chemical mapping due to the processed data consisting as an array of square shaped

pixels. Many domains in pharmaceutical tablets are irregular in shape and errors associated with the inability to characterise round objects will therefore be minimised when analysing real pharmaceutical products. 3D filtering using the Mean Filter did however slightly increase the error in the surface area of the AmberLite™ bead; however, this difference is insignificant and may have resulted from over smoothing.

3.3 | 3D Raman mapping investigation for the simplified model system

To determine the capability of 3D chemical imaging for pharmaceutical samples, our proposed 3D Raman mapping method was applied to a model formulation. A three-component model system composed of an API (eletriptan hydrobromide, $C_{22}H_{27}BrN_2O_2S$), a common diluent (MCC, $C_{14}H_{26}O_{11}$) and a secondary excipient (saccharin, $C_7H_5NO_3S$) in a 1:1:1 w/w ratio was used to simulate a drug product. All materials are pharmaceutically relevant and differed in their chemical (Raman response) and physical (particle size and shape) properties. The structures of each material, their respective Raman spectra and SEM micrographs demonstrating the raw materials primary particle size and shape are displayed in Figure S2.

3.3.1 | 3D chemical image reconstruction

A depth interval of 30 μm was chosen for this experiment due to being smaller than the primary particle size of the smallest component, eletriptan hydrobromide (40 μm), and therefore, all domains should be visualised in the 3D image (Figure S7). The resultant 3D dataset (Figures S3–S6) consisted of large networks of agglomerated particles due to the high composition of each component. Particle networks are notoriously difficult to characterise, and more valuable information regarding the size, shape and position of domains can be determined from discrete particles.

To evaluate the true capabilities of 3D Raman mapping for pharmaceutical solid dosage forms, a new composition, more typical to a real pharmaceutical drug product, was devised. The new formulation consisted of MCC, saccharin and eletriptan hydrobromide in a 0.80:0.15:0.05 w/w ratio, respectively. MCC is the most widely used direct compaction excipient and is classified as a primary excipient.^{36,37} Its role as a binding agent requires it to be the major component in many formulations. Secondary excipients, used to make robust formulations, such as saccharin, are typically present as one of

TABLE 2 A comparison of the diameter calculated and 3D Object Counter calculated values for the AmberLite™ Na Ion Exchange Resin bead for the raw and filtered datasets

	Volume/ $\times 10^6 \mu\text{m}^3$	Surface Area/ $\times 10^4 \mu\text{m}^2$
Diameter calculated	10.5	23.2
Raw data	8.32	29.3
3D Gaussian Blur	8.44	29.3
3D Mean Filter	8.46	30.2

the minor components within a formulation. APIs are usually only present in small quantities, typically less than 10% for most formulations.

For the new formulation, Raman spectroscopic chemical images were collected at 20 μm depth intervals into the sample to obtain more detailed morphological information on the size and shape of domains. The previous 3D experiment on the three-component model system demonstrated that using our proposed milling procedure with a polishing step size of 2 μm , it was possible to accurately remove 20 μm while still obtaining an optically flat surface suitable for Raman mapping.

The reconstructed 3D volumetric Raman map of the new formulation is displayed in Figure 6a. The individual 2D chemical images used for the 3D reconstruction can be found in Figure S8. The 3D volume shows the major component (MCC) exists as a large network domain of

agglomerated particles, and 3D visualisation does not provide any further information regarding domain size or shape. To better visualise the 3D size and shape of the lower concentration components, the major component was removed from the 3D volume (Figure 6b). All eletriptan hydrobromide and saccharin domains can be visualised in this representation and reveal that the majority of eletriptan hydrobromide domains are adjacent to saccharin domains. The 3D visualisation enables an enhanced understanding regarding the association of the two components within the 3D tablet matrix. The 2D chemical images (Figure S8) show some association; however, due to only examining single XY planes, adjacency in an orientation other than the XY plane cannot be identified.

The 3D chemical image can also be visualised as an orthoslice, displayed in Figure 7a. The orthoslice

FIGURE 6 A 3D volumetric representation of the distribution of MCC (blue), saccharin (green) and eletriptan hydrobromide (red) reconstructed using FIJI 3D Viewer³⁴ [Colour figure can be viewed at wileyonlinelibrary.com]

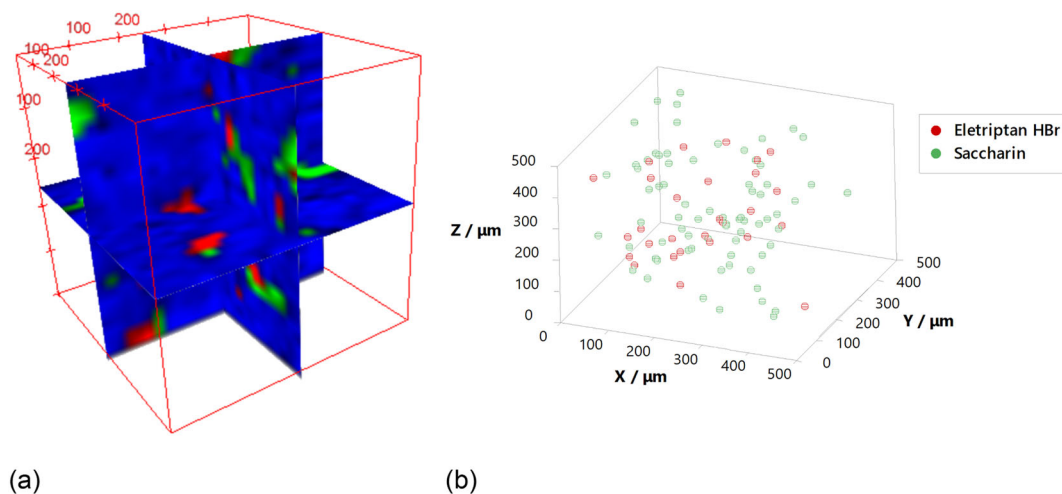
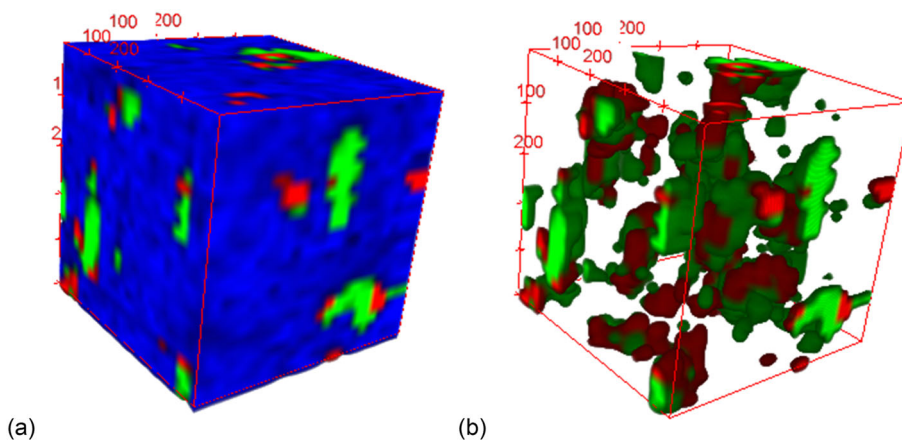


FIGURE 7 (a) A 3D orthoslice representation of the distribution of MCC (blue), saccharin (green) and eletriptan hydrobromide reconstructed using FIJI 3D Viewer³⁴ (red) and (b) a 3D scatterplot of the geometric centres of eletriptan hydrobromide and saccharin domains calculated using FIJI 3D Object Counter³⁵ [Colour figure can be viewed at wileyonlinelibrary.com]

representation enables slices orthogonal to the XY plane to be extracted enabling the 3D visualisation of domains within the core of the sample dataset.

The 3D Object Counter plugin³⁵ was used to obtain 3D domain size statistics for the eletriptan hydrobromide and saccharin domains. 3D visualisation of the geometric centres of each component domains, shown in Figure 7b, further demonstrates the association between the two components within the tablet matrix. By determining the geometric centres of each component domains, differences in the size of domains and arrangement of components across datasets can be easily identified and visualised in 3D.

The number, average volume and surface area of the eletriptan hydrobromide and saccharin domains were also calculated and are displayed in Table S1. Quantification of these values may be more useful as a comparison tool to assess relative differences in the size and distribution of domains across components and samples. The effect of processing and compaction conditions on the size, shape and distribution of components may be better understood and may be used to optimise current manufacturing processes. Alternatively, relative differences in the morphology of a component's domains may be useful to identify the root cause of OOS batches.

4 | CONCLUSIONS

This research successfully demonstrated that our proposed 3D chemical mapping method can be used to visualise the 3D structure of a solid dosage form sample of interest. The AmberLite™ validation study examined spherical shaped objects, which are known to be the most difficult shaped objects to characterise via chemical mapping, and we were still able to obtain useful qualitative and quantitative data within an acceptable error. All limitations and errors discussed for our method are systematic and therefore consistent across all datasets if method parameters remain constant. Therefore, this method can be used to determine relative differences in the size and shape of domains across components or datasets to provide an enhanced understanding of the 3D structure of tablet system. Performing 3D domain size statistics enables quantitative differences in the size, shape and distribution of domains across samples or components to be obtained. Quantification of these differences can provide a powerful insight when analysing pharmaceutical tablets to characterise how materials may change during processing and compaction conditions or to understand OOS batches. The majority of domains within pharmaceutical tablets are irregular in shape, which are easier to characterise via chemical mapping.

Due to the long data acquisition times required to build a 3D Raman image of a tablet matrix, we believe this method is most suited to baselining the 3D structure of new pharmaceutical tablets prior to being commercialised. By fully understanding the desired 3D size and arrangement of components within a tablet system, the effect of each manufacturing process on the formulation can also be better understood. Technology transfers from development to manufacturing or to alternative manufacturing sites may be easier to achieve. The root cause of OOS samples may be more quickly identified to a single manufacturing step minimising the disruption in drug supply to patients in need. Despite the added value of 3D Raman mapping, 2D chemical mapping is still a useful tool to rapidly characterise differences in the spatial distribution of components in troubleshooting investigations. Ultimately, the choice of imaging method for a particular formulation will depend on the time availability for analysis, the homogeneity of the sample and the information that is required for the study.

ACKNOWLEDGEMENT

This work was supported by Global Technology and Engineering, Pfizer Global Supply.

CONFLICT OF INTEREST

The authors declare that they have no conflicts of interest.

DATA AVAILABILITY STATEMENT

All data underpinning this publication are openly available from the University of Strathclyde KnowledgeBase at: <https://doi.org/10.15129/9c893711-a273-42f5-960c-33c5daa0ab24>.

ORCID

Hannah Carruthers  <https://orcid.org/0000-0003-1702-4351>

Karen Faulds  <https://orcid.org/0000-0002-5567-7399>

Duncan Graham  <https://orcid.org/0000-0002-6079-2105>

REFERENCES

- [1] L. Allen, H. C. Ansel, *Ansel's Pharmaceutical Dosage Forms and Drug Delivery Systems*, Wolters Kluwer, Baltimore **2013**.
- [2] C. B. Hancock, M. P. Mullarney, *Pharm. Technol.* **2005**, 29, 44.
- [3] C. Gendrin, Y. Roggo, C. Collet, *J. Pharm. Biomed.* **2008**, 48, 3.
- [4] A. V. Ewing, S. G. Kazarian, *Spectrochim. Acta, Part A.* **2018**; 197, 2018, 197, 10.
- [5] H. Carruthers, D. Clark, F. Clarke, K. Faulds, D. Graham, *Appl. Spectrosc.* **2021**, 75, 2.
- [6] T. Frosch, E. Wyrwich, D. Yan, J. Popp, T. Frosch, *Molecules* **2019**, 24, 23.

- [7] H. Hisada, A. Okayama, T. Hoshino, J. Carriere, T. Koide, Y. Yamamoto, T. Fukami, *Chem. Pharm. Bull.* **2020**, *68*, 2.
- [8] M. Y. Fujii, Y. Yamamoto, T. Koide, M. Hamaguchi, Y. Onuki, N. Suzuki, T. Suzuki, T. Fukami, *Appl. Spectrosc.* **2019**, *73*(10), 1192.
- [9] A. A. Gowen, C. P. O'Donnell, P. J. Cullen, S. E. Bell, *Eur. J. Pharmacol.* **2008**, *69*, 1.
- [10] S. Šašić, W. Yu, L. Zhang, *Anal. Methods* **2011**, *3*, 3.
- [11] C. Gendrin, Y. Roggo, C. Collet, *Talanta* **2007**, *73*(4), 741.
- [12] D. Clark, M. Henson, F. LaPlant, S. Šašić, L. Zhang, in *Pharmaceutical Applications of Mapping and Imaging in Handbook of Vibrational Spectroscopy*, (Eds: D. E. Pivonka, J. M. Chalmers, P. R. Griffiths), Wiley, London **2007** 309.
- [13] D. Clark, S. Šašić, *Cytom. J. Int. Soc. Anal. Cytol.* **2006**, *69*, 8.
- [14] S. Šašić, A. Kong, G. Kaul, *Anal. Methods* **2013**, *5*, 9.
- [15] N. Everall, *Spectroscopy* **2004**, *19*, 19(10), 22.
- [16] N. Everall, *Spectroscopy* **2004**, *19*(11), 16.
- [17] M. Gu, *Principles of Three-Dimensional Imaging in Confocal Microscopes*, World Scientific, Victoria **1996**.
- [18] Y. Yamamoto, M. Y. Fujii, T. Fukami, T. Koide, *J. Drug Deliv. Sci. Technol.* **2019**, *51*, 639.
- [19] T. Schäfer, R. E. Di Paolo, R. Franco, J. Crespo, *Chem. Commun.* **2005**, *20*, 2594.
- [20] M. J. Matthews, A. L. Harris, A. J. Bruce, M. J. Cardillo, *Rev. Sci. Instrum.* **2000**, *71*(5), 2120.
- [21] S. Nakashima, *J. Phys.* **2003**, *16*(2), S37.
- [22] N. Everall, *J. Raman Spectrosc.* **2014**, *45*, 1.
- [23] N. Everall, *Analyst* **2010**, *135*, 10.
- [24] N. Everall, *Appl. Spectrosc.* **2009**, *63*, 9.
- [25] R. C. Rowe, P. Sheskey, M. Quinn, *Handbook of Pharmaceutical Excipients*, Academic Press, London **2009**.
- [26] T. Böhm, R. Moroni, S. Thiele, *J. Raman Spectrosc.* **2020**, *51*, 1160.
- [27] F. Muzzio, S. Panikar, *Am. Pharm. Rev.* **2016**, *19*, 6.
- [28] F. Muzzio, S. Panikar, *Powder Bulk Eng.* **2016**, *1*, 62.
- [29] S. Gupta, T. Omar, F. J. Muzzio, *Int. J. Pharm.* **2022**, *611*, 121331.
- [30] F. C. Clarke, M. J. Jamieson, D. A. Clark, S. V. Hammond, R. D. Jee, A. C. Mofatt, *Anal. Chem.* **2001**, *73*, 10.
- [31] G. Socrates, *Infrared and Raman Characteristic Group Frequencies: Tables and Charts*, Wiley, Chichester **2002**.
- [32] J. Schindelin, I. Arganda-Carreras, E. Frise, V. Kaynig, M. Longair, T. Pietzsch, S. Preibisch, C. Rueden, S. Saalfeld, B. Schmid, J. Y. Tinevez, D. J. White, V. Hartenstein, K. Eliceiri, P. Tomancak, A. Cardona, *Nat. Methods* **2012**, *9*, 7.
- [33] C. A. Schneider, W. S. Rasband, K. W. Eliceiri, *Nat. Methods* **2012**, *9*, 7.
- [34] B. Schmid, J. Schindelin, A. Caronda, M. Longair, M. Heisenberg, *BMC Bioinform.* **2010**, *11*, 1471.
- [35] S. Bolte, F. P. Cordelières, *J. Microsc.* **2006**, *224*, 213.
- [36] Y. Zhang, Y. Law, S. Chakrabarti, *AAPS PharmSciTech* **2003**, *4*, 4.
- [37] G. Thoorens, F. Krier, B. Leclercq, B. Carlin, B. Evrard, *Int. J. Pharm.* **2014**, *473*, 473.

SUPPORTING INFORMATION

Additional supporting information may be found in the online version of the article at the publisher's website.

How to cite this article: H. Carruthers, D. Clark, F. C. Clarke, K. Faulds, D. Graham, *J Raman Spectrosc* **2022**, *1*. <https://doi.org/10.1002/jrs.6337>